Study of post-impact behaviour of thin hybrid carbon/epoxy and glass/epoxy woven composite laminates under fatigue tensile loading – Part II: Numerical study

A. Rogani, Pablo Navarro, Steven Marguet, Jean-François Ferrero, C. Lanouette

Study of post-impact behaviour of thin hybrid carbon/epoxy and glass/epoxy woven composite laminates under fatigue tensile loading - Part II : numerical study

A. Rogani[a,b], P. Navarro[a], S. Marguet[a], J-F. Ferrero[a], C. Lanouette[b]

[a] *Université de Toulouse, Institut Clément Ader, FRE CNRS 3687, UPS/INSA/ISAE/Mines Albi, 3 rue Caroline Aigle, 31400 Toulouse, France*
[b] *Airbus Helicopters, 1 Place du Générale Valérie André, 93440, Dugny, France*

Abstract

This article concerns the modelling of post-impact damage propagation in thin carbon/epoxy and glass/epoxy hybrid woven composite laminates loaded in fatigue tension. The modelling is based on the semi-continuous approach implemented into the explicit finite element code RADIOSS. The bundles are modelled with rod elements and the resin is modeled with a specific damageable shell element, used to stabilize the bundles. This approach is extended to post-impact fatigue tensile loadings. Resin damaging is implemented for the shell elements through two fatigue laws $Y_{xy} - N_{resin\,a}$ and $Y_{xy} - N_{resin\,b}$ based on thermodynamical forces and identified through the experimental results obtained in Part I. Fiber breakage is introduced for rod elements through Basquin curves based on tensile and compressive strains. The damage accumulation is taken into account by a Miner's rule. For several impact energies and amplitude of fatigue loading, the modelling well correlates the experimental results in terms of damage propagation scenario, path and speed.

Preprint submitted to Composite Structures *November 6, 2020*

Keywords: Fatigue, Woven composites, thin laminates, hybrid laminates, post-impact behaviour, explicit F.E modelling, semi-continuous approach, damage

---

1. Introduction

This article deals with the modelling of post-impact damage propagation in thin hybrid carbon/epoxy and glass/epoxy woven composite laminates under fatigue tensile loading. In this paper, the semi-continuous approach, already validated for quasi-static tensile loading on mono-material and hybrid woven composite laminates in [1], is extended to fatigue loading. It is the second second part of a two-parts article : the phenomenons which occur during the fatigue tensile test have been investigated through several experimental tests. They are described in Part I.

The damage generated by an impact on a woven composite structure is typically composed of matrix cracking, delamination and fibre breakage. When the structure is subject to fatigue tensile loading, these types of damage propagate, what leads to the final failure of the structure. In order to optimize the post-impact behaviour of their woven composite structure without expensive testings campaigns, the aeronautical industries try to develop numerical tools able to predict the damage propagation.

However, the literature on the subject is barely existing. Most of the studies have been conducted on laminates with an initial defect such as notches, holes or delamination. In these cases, the resin damaging is modeled through a continuum damage modelling (CDM) [2, 3]. This approach has been introduced in quasi-static for non-damaged unidirectional composite laminates by Talreja, Ladevèze and LeDantec [4, 5]. The principle is to come degrade the stiffness matrix by one or some damage variables, calculated through thermodynamical forces. Hochard et al. [6, 7, 2, 3] have adapted this approach to carbon woven composites in quasi-static [6, 7] and in fatigue [2, 3].

They have introduced a fatigue damage variable depending on the variation of thermodynamical forces on one fatigue cycle and the number of cycles. Moreover, they have introduced a threshold value corresponding to the minimal thermodynamic force necessary to initiate matrix crackings. A similar modelling (Onera Damage modelling) has been developed by the ONERA, especially for organic matrix and 3D woven [8, 9]. Their modelling takes into account thermal strains and viscoelasticity. In fatigue, the damage variable includes a static part and a damaging accumulation. For that, they have two modulus : first a static modulus for the static rise which creates a resin damaging and then a fatigue modulus which increases this damaging depending on the number of cycles. Then the variables are updated and the calculation comes back to the static modulus to evaluate the residual performances of the laminate.

To propagate fibers breakages in a glass/woven composite laminate, Rouault [10] based on $\varepsilon - N$ curves of its woven fabric identified on fatigue testings on non-impacted samples. He calculates the strains in each element of its modelling. With the curve, he knows the number of cycles necessary to break each element. Then, the principle is delete the element which requires the lower number of cycle to reach the failure. In this case, the damage accumulation is taken into account with a Miner's rule [11]. Some authors use empirical criterions as the point stress criterion (PSC) and the average stress criterion (ASC). They have been introduced by Whitney and Nuismer [12]. They observed that, for holed laminate, the maximal stress at the edge of the hole in fatigue can overtake the quasi-static maximal stress without damage propagation. For the PSC, the stress to evaluate the damage propagation

is calculated at a distance d_0 f the hole. For the ASC, the stress is a mean stress calculated along a distance d_0. Tan et al. [13] used the PSC method to evaluate the stress at failure of samples with an elliptical hole. Miot [2] used the ASC method for holed and notched carbon laminates. She uses a characteristic volume in order to calculate a mean stress and evaluate the damage propagation. But, even if the implementation of these criterions is simple, they are very dependant on the testings parameters.

Concerning the delamination modelling, cohesive elements are a lot used for impact loading. Their concept have been introduced by Hillerborg et al. [14]. A cohesive law links the stress state in the element with the relative displacement of the nodes and a critical energy release rate G_c manages the dissipated energy in the cracking opening. Robinson et al. [15] used them to model the propagation of delamination in fatigue. They represent the delamination propagation in fatigue as a combination of the propagation due to the amplitude of the static loading and due to the cyclic repetition of the load. To do that, they introduce a fatigue damage variable in addition to the damage variable of the classic law. It depends on the relative displacement of the nodes ans the number of cycles.

Some authors use the cohesive elements to model the propagation of matrix crackings. For example, Hallett et al. [16] used them for a tensile simulation on a holed sample. For this purpose, they have first noted the position of the crackings after an experimental test. Then, they meshed the sample placing the cohesive elements on potential paths of the crack propagation.

The objective of the study is to model fatigue tensile tests on impacted woven laminates with the semi-continuous approach [17, 18, 19, 20, 21, 1].

For this purpose, the existing semi-continuous strategy has been improved. In fact, add-ons, based on experimental observations made in Part I, are introduced through propagation laws in fatigue of resin damaging (tows/resin splittings and intra-tows crackings) and fibres breakages. A calculation strategy has been implemented in order to perform their propagation in the explicit finite element code Radioss. The model is calibrated and validated, for several impact energies and levels of solicitation, by simulations on the same woven laminates used in Part I (Tables 1-2).

2. Semi-continuous modelling in quasi-static tension

2.1. Presentation

In this study, the semi-continuous modelling is extended to fatigue tensile simulation. It has been developed in the research team for impact loadings [17, 18, 19, 20] and extended to post-impact quasi-static tensile loadings on woven laminates [1] into the explicit finite element code Radioss.

The modelling strategy is to decouple the resin and tows behaviour in order to represent simultaneously the damaged resin and the undamaged fibers tows (Figure1). For this purpose, a specific finite element is developed. It is made up a truss structure of rod elements, modeling the woven fabric bundles and following the woven pattern geometry, and a shell element, representing the epoxy matrix. An interface element, with an elasting damaging behaviour based on a bilinear cohesive law, connects two plies and represent the delamination.

The rod elements have an elastic and brittle behaviour. Their breakage

are calculated through tensile and compressive strain criterions :

$$\text{If } \varepsilon(x) > \varepsilon_{max}^{tension} \text{ or } |\varepsilon(x)| > |\varepsilon_{max}^{comp}| \text{ then break of the bar element} \qquad (1)$$

Furthermore, the cross-point of the woven ply are taken into account for these criterions. Indeed, at a cross-point, the fibres bundles are in local bending. So, they need a more (*resp. less*) important tensile (*resp. compressive*) strain to spread out and reach the tensile (*resp. compressive*) strain criterion. So, at a cross-point, $\varepsilon_{max}^{tension}$ is increased and $|\varepsilon_{max}^{comp}|$ is reduced. For this purpose, $\varepsilon_{max\,cross}^{comp}$ and $\varepsilon_{max\,cross}^{tension}$ are introduced in the model such as :

$$\frac{|\varepsilon_{max\,cross}^{comp}|}{|\varepsilon_{max}^{comp}|} = \frac{\varepsilon_{max}^{tension}}{\varepsilon_{max\,cross}^{tension}} \qquad (2)$$

The resin has an elastic and isotropic behaviour with an anisotropic damaging in each direction of the woven through two damage variables d_1 and d_2, based on thermodynamical forces (or energy release rates). It has also a pseudo-plastic behaviour in plane shear with a shear damaging law. It is calculated through two damage variables d_{xy}^a and d_{xy}^b which represent respectively tows/resin splittings and cracks into bundles [1]. This original shear damaging law is based on experimental observations made by [22, 23] during quasi-static tensile tests on carbon/epoxy woven laminate oriented at $\pm 45^\circ$: first there is an initiation of tows/resin splitting and then, intra-tows crackings initiate and propagate in meta-delamination (delamination between warp and weft bundles). The splittings quickly evolve at the beginning of the test then they stabilize. The crackings and the meta-delaminations slowly grow at the beginning and suddenly accelerate once the splittings no longer evolve. However, the modelling scale is not enough small to represent

meta-delamination. The two damage variables depend on thermodynamical function, as it is commonly used [7, 3] :

$$\begin{cases} d_{xy}^{a} = d_{xy}^{a\,max} \times \left(1 - exp\left(-\dfrac{\langle\sqrt{Y_{xy}} - \sqrt{Y_0}\rangle_{\geq 0}}{\sqrt{Y_c}}\right)\right) \\ \\ d_{xy}^{b} = max\left(exp\left(\dfrac{\langle\sqrt{Y_{xy}} - \sqrt{Y_{0\,bis}}\rangle_{\geq 0}}{\sqrt{Y_{c\,bis}}}\right), 1\right) \end{cases} \tag{3}$$

where Y_0 (respectively $Y_{0\,bis}$) and Y_c (respectively $Y_{c\,bis}$) are parameters of damage threshold and damage speed of d_{xy_a} (respectively d_{xy_b}). $d_{xy_a}^{max}$ is the maximal limit of d_{xy_a}. This limit has been introduced for tows/resin splittings because they are not responsible for the final break of the laminate.

The coupling of the shear stress with the stresses in the other directions is neglected. So, shear strain energy is only due to shear stress and the thermodynamical function Y_{xy} is defined by :

$$Y_{xy} = \frac{\partial W_{xy}}{\partial d_{xy}} \tag{4}$$

where $d_{xy} = d_{xy}^{a} + d_{xy}^{b}$ and W_{xy} is the shear strain energy defined by :

$$W_{xy} = \frac{\tau_{xy}^{2}}{2G_{xy}^{0}(1 - d_{xy})} \tag{5}$$

Hence :

$$Y_{xy} = \frac{1}{2} G_{xy}^{0} \gamma_{xy}^{e\;2} \tag{6}$$

Finally, the two shear damage variables are used to degrade the shell and the bending matrix :

$$\begin{bmatrix} \dfrac{(1-d_1)\left(1-d_{xy}^{a}-d_{xy}^{b}\right)E_1}{1-(1-d_1)(1-d_2)\left(1-d_{xy}^{a}-d_{xy}^{b}\right)\nu_{xy}\nu_{21}} & \dfrac{(1-d_1)(1-d_2)\left(1-d_{xy}^{a}-d_{xy}^{b}\right)\nu_{21}E_1}{1-(1-d_1)(1-d_2)\left(1-d_{xy}^{a}-d_{xy}^{b}\right)\nu_{xy}\nu_{21}} & 0 \\ \dfrac{(1-d_1)(1-d_2)\left(1-d_{xy}^{a}-d_{xy}^{b}\right)\nu_{xy}E_2}{1-(1-d_1)(1-d_2)\left(1-d_{xy}^{a}-d_{xy}^{b}\right)\nu_{xy}\nu_{21}} & \dfrac{(1-d_2)\left(1-d_{xy}^{a}-d_{xy}^{b}\right)E_2}{1-(1-d_1)(1-d_2)\left(1-d_{xy}^{a}-d_{xy}^{b}\right)\nu_{xy}\nu_{21}} & 0 \\ 0 & 0 & \left(1-d_{xy}^{a}-d_{xy}^{b}\right)G_{xy}^{0} \end{bmatrix}$$

The irreversible strains are taken into account by the introduction of a pseudo-plastic criterion on the in-plane shear stress based on an isotropic hardening using a classic elastic prediction and a plastic correction. An elastic field is defined by :

$$f = |\tau_{xy}| - K_{plas} p^{\beta} - \tau_0 \tag{7}$$

where τ_{xy} is the in-plane shear stress, τ_0 is the plastic strength, (K_{plas}, β) are parameters of the plastic hardening law and p the cumulative plastic strain. Thus, if $f > 0$, the plastic correction is performed through the update of the plastic variables γ_{xy}^{p} and p, based on a Newton-Raphson iterative scheme, with γ_{xy}^{p} the plastic shear strain defined by :

$$\gamma_{xy} = \gamma_{xy}^{e} + \gamma_{xy}^{p} \tag{8}$$

where γ_{xy} is the total shear strain and γ_{xy}^{e} is the elastic shear strain.

2.2. Validation

The semi-continuous modelling has been validated in quasi-static for all the mono-material and hybrid woven laminates presented in the Tables 1-2 [1]. The model well represents the propagation of the post-impact damage. The fracture surfaces and the load - crosshead displacement curves well correlate the experimental results.

3. Propagation laws in fatigue

3.1. Resin damaging

The fatigue tensile loadings on impacted samples of configuration C45C45 and C0C0, performed in Part I, have shown that the post-impact damage

propagation was governed by shear damaging : tows/resin splittings and intra-tows crackings propagate in the laminate at $\pm 45°$ for the configuration C45C45 and vertically for the configuration C0C0. In both cases, the two resin damaging types follow the same direction and have a similar behaviour. But, the splittings emerge first and propagate faster than the crackings.

As for the quasi-static modelling, the propagation in fatigue of each type of resin damaging is based on thermodynamical forces. Two fatigue laws $Y_{xy} - N_{resin\,a}$ and $Y_{xy} - N_{resin\,b}$ are implemented for the shell element, only for carbon material. $N_{resin\,a}$ and $N_{resin\,b}$ are the number of cycles necessary to initiate respectively the tows/resin splittings and the intra-tows crackings. They are expressed as Basquin curves :

$$N_{resin\,a} = \left(\frac{Y_a}{Y_{xy} - Y_a^0} \right)^{\frac{1}{\alpha}} \quad and \quad N_{resin\,b} = \left(\frac{Y_b}{Y_{xy} - Y_b^0} \right)^{\frac{1}{\beta}} \tag{9}$$

where Y_a, α, Y_b and β are parameters of the fatigue laws. Threshold values Y_a^0 and Y_b^0 have also been added for each damage type [2, 3]. These parameters will be identified through severeal post-impact fatigue tensile simulations on laminates C45C45 and C0C0.

3.2. Fibres bundles breakages

The fatigue tensile loadings on impacted samples of configuration G0G0, G0C45C45 and G0C45C0, performed in Part I, have shown fibres bundles breakages in carbon and glass plies. They are taken into account in the semi-continuous modelling through the implementation of two Basquin curves (for each material) for the rod elements based on their tensile strain :

$$N_{breakage\,bundle} = \left(\frac{\varepsilon_6^{tension}}{\langle \varepsilon_{bundle} \rangle_+} \right)^{\frac{1}{\gamma}} \tag{10}$$

where $\langle \varepsilon_{bundle} \rangle_+$ is the tensile strain of the rod element during the simulation. $\varepsilon_{6^{tension}}$, the tensile strain at 10^6 cycles, and γ are the law parameters. They have been identified by Airbus Helicopters by tensile fatigue testings piloted in strain on non-impacted samples of configuration C0C0 and G0G0. In fact, in tension, the sample behaviour is governed by the fibres.

The tensile loadings on impacted samples of configuration G0C45C45, performed in [21] and Part II, indicate a similar behaviour in quasi-static and fatigue. In the glass ply, the damage propagation is due to tensile and compressive breakage of warp and weft bundles [21, 1]. In fact, the glass ply elongation is piloted by the two carbon plies elongation. So, the weft bundles of the glass ply are compressed due to the Poisson's effect of the carbon plies oriented at $\pm 45°$. In the quasi-static modelling, this phenomenon is represented by a compressive strain criterion of the rod element (see 2.1).

In fatigue, this phenomenon is represented by the introduction of a Basquin curve for the rod elements based on their compressive strain :

$$N_{breakage\,bundle} = \left(\frac{|\varepsilon_6^{comp}|}{|\langle \varepsilon_{bundle} \rangle_-|} \right)^{\frac{1}{\gamma}} \tag{11}$$

where $\langle \varepsilon_{bundle} \rangle_-$ is the compressive strain of the rod element during the simulation. The value of γ is the same as in tension. ε_6^{comp} is chosen such as the ratio $|\varepsilon_6^{comp}|/\varepsilon_6^{tension}$ is the same as in quasi-static :

$$\frac{|\varepsilon_6^{comp}|}{\varepsilon_6^{tension}} = \frac{|\varepsilon_{max}^{comp}|}{\varepsilon_{max}^{tension}} \tag{12}$$

The cross-points are also taken into account in fatigue. In fact, the experiments of Part I have indicated than the propagation of glass fibres breakages

in the impacted laminates of configuration G0G0 and G0C45C45 was guided by the cross-points of the woven plies. In tension and compression, two different curves are used whether the fibre is located at a cross-point or not such as :

$$\frac{\varepsilon_6^{tension}}{\varepsilon_{6\,cross}^{tension}} = \frac{|\varepsilon_{6\,cross}^{comp}|}{|\varepsilon_6^{comp}|} = \frac{\varepsilon_{max}^{tension}}{\varepsilon_{max\,cross}^{tension}} \tag{13}$$

3.3. Damage accumulation

The damage accumulation in the shell and rod elements during the fatigue tensile simulation is take into account by a simple Miner's rule. For each rod element and shell element of the specific woven finite element (Figure 1), a variable D_m is introduced such as :

$$D_m = \sum_i \frac{n_i}{N_i} \tag{14}$$

For a rod element, n_i is the number of cycles realized at a strain ε_i for which the number of cycles at failure is N_i. For a shell element, n_i is the number of cycles realized at an energy release rate Y_i for which the number of cycles at failure is N_i. Thus, if $D_m = 1$, the rod or the shell element is deleted.

4. Strategy of post-impact fatigue tensile simulation

4.1. Principe

The principle of the simulation strategy is to find in the model the rod or the shell element which requires the lowest number of cycles to break. That amounts to find the number of cycles N_{elem} which verifies :

$$N_{elem} = \min_{j \in mesh} \left[(1 - D_m(j)) * \left(\frac{\varepsilon_6}{\varepsilon_j} \right)^{\frac{1}{\gamma}}, (1 - D_m(j)) * \left(\frac{Y_i}{Y_j - Y_i^0} \right)^{\frac{1}{k}} \right] \tag{15}$$

with $i = a$ or b and $i = \alpha$ or β.

4.2. Strategy

Finally, the post-impact fatigue tensile simulation strategy is implemented in FORTRAN through a user law in the explicit finite element code Radioss. The user law is made up of a quasi-static and a fatigue modules. The steps of the simulation are :

1. A quasi-static rise is numerically realized until the maximum displacement of the experimental fatigue cycle : $\Delta L = \Delta L_{sta} + \Delta L_{dyn}$. A first calculation of the strains and the thermodynamical forces are performed for each element of the model.

2. Then, the calculation goes into the fatigue module :

   (a) First, the breakage number of cycles à rupture is calculated for each rod element and shell element (only for carbon) of the model.

   (b) If the lowest number of cycles is reached for :

   - a rod element : then it is deleted of the model as well as the shell element. Indeed, it assumed that the bundle breakage lead to the breakage of the resin in the bundle and at the interface between the bundle and the resin.

   - a shell element : either the damage corresponds to tows/resin splitting so the shell element does not have to be entirely deleted because the intra-tows crackings did not appear yet.

The damage variable of the shell element is set to 0.5. Or the damage corresponds to intra-tows crackings and the shell element is entirely deleted.

(c) Once the rod or the shell element is damaged, the number of cycles and all the variables D_m (in order to simulate the damage accumulation) are uploaded.

3. Before moving to the next iteration, the calculation goes again into the quasi-static module in order to get the new strains and thermodynamical forces of each element of the model.

5. Fatigue tensile simulations on impacted samples

5.1. Identification and validation on mono-material laminates

5.1.1. Introduction

In this part, the propagation laws presented above are identified and validated on the mono-material laminates. For the tows/resin splittings and the intra-tows crackings, they are identified and validated through simulations on samples of configuration C45C45 and C0C0. For glass fibres breakages, they are validated through simulations on samples of configuration G0G0. The objective is to obtain numerical results which well correlate the experimental results in terms of damage propagation scenario, damage propagation velocity and number of cycles at failure. In order to test the robustness and the validity of the modelling, the same impact energies and displacement levels as in the experimental study are used for the simulations. They are presented on the Table 3.

5.1.2. Configurations C0C0 and C45C45

The propagation laws in fatigue $Y_{xy} - N_{cycles}$, identified for the tows/resin splittings and the intra-tows crackings, are presented on the Figure 2.

Configuration C45C45.

For the configuration C45C45, the post-impact damage scenario is presented on the Figure 3. As for the experimental testings, the damage propagates at $\pm 45°$. Tows/resin splittings initiate from each tip of the initial damage transversely to the initial fibres breakages. They join into a unique point and form a rhombus-shape damage. Then, they propagate at $\pm 45°$ from this point. Once this propagation is started, intra-tows crackings initiate also and propagate at $\pm 45°$ following the tows/resin splittings. Their propagation continue with a slower progression of the intra-tows crackings. Finally, the splittings reach the edges of the samples following some cycles later by the intra-tows crackings. The samples is entirely cracked on a $\pm 45°$ band. The numbers of cycles required to reach the edges of samples obtained with the modelling are very close to the values experimentally obtained (Tables 4-5).

For the couples (ΔL_2 ; 2.25 J) and (-20% ΔL_2 ; 4 J), the post-impact damage barely propagates (Figure 4). In fact, the values of energy release rates calculated in the sample are lower than the value required to initiate intra-tows crackings (Figure 5). So, they need a high number of cycles to emerge.

Configuration C0C0.

For the laminate C0C0, the post-impact damage propagation scenario

obtained with the modelling is in accordance with the experimental results obtained in Part I. Tows/resin splittings and then intra-tows crackings propagate vertically during the fatigue simulation (Figure 6).

Furthermore, the velocity of damage propagation numerically obtained well correlates the velocity experimentally obtained. The evolution curves depending on the number of cycles are presented on the Figure 7 for the tows/resin splittings and then intra-tows crackings. They are close to the experimental curves for all the energies and displacement levels tested.

They propagate out of step very quickly in the 100 000 - 200 000 first cycles before stabilizing progressively. This stabilization is due to the decrease of the shear strains in the resin at the tip of the damage propagation as the simulation progresses. That leads to a decrease of the energy release rates in the resin and an increase of the number of cycles required to initiate the splittings. Finally, for 10^7 cycles, the energy release rates calculated at the tip of the splittings are lower to the damages threshold values Y_0^a and Y_0^b. So, the damage no longer evolves

For the highest displacement level (+30% ΔL_3), the fibres reach their quasi-static tensile strain criterion during the quasi-static rise. That leads to an horizontal propagation of fibres breakages as in quasi-static (Figure8) [1].

5.1.3. Configuration G0G0

For the configuration G0G0, the fracture surface numerically obtained for each impact energy and displacement level is in accordance with the experimental results (Figure 9). Fibres breakages propagate horizontally following the cross-points of the woven fabric (Figure 10).

The damage propagation initiation and speed are close to those experimentally obtained. Indeed, the experimental and numerical curves of damage length depending on the number of cycles have the same appearance (Figure 11) and the number of cycles at the sample failure are close.

5.1.4. Conclusion

The semi-continuous modelling is validated for the mono-material laminates. For C45C45, C0C0 and G0G0, the model well correlates the experimental results of Part I in terms of damage propagation scenario, damage propagation velocity and number of cycles at failure for several impact energies and displacement levels.

In the next part, the semi-continuous modelling is tested on the hybrid configuration G0C45C45.

5.2. Validation on hybrid laminate G0C45C45

As for the mono-material configurations, several impact energies and displacement levels are tested for G0C45C45. The values are presented in the Table 6.

For each impact energy and displacement level, the fracture surfaces are in accordance with the experimental results of Part I (Figure 12). Fibres breakages propagate at $\pm 45^{\circ}$ following the cross-points of the upper glass ply (Figure 13) and and resin damaging propagates at $\pm 45^{\circ}$ in the lower carbon ply.

The post-impact damage propagation scenario is precisely obtained (Figure 14) . The simulation brings some elements not visible during the experimental tensile tests in Part I. Fibres breakages initiate in the upper glass

ply while no resin damaging has emerged in the two carbon plies. Warp and weft bundles are highly loaded respectively in tension and compression at the tip of the damage propagation. That leads to a propagation a fibres breakages in tension for warp bundles and in compression for weft bundles. They propagate at $\pm 45^{\circ}$ following the cross-points of the glass ply along an area highly loaded in plane-shear in the carbon plies. In fact, the carbon plies elongation pilots the glass ply elongation. Fibres breakages propagate gradually in the glass ply and, out of step, resin damaging propagates also in the carbon plies. From a certain number of cycles, the splittings in carbon plies overtakes the fibers breakages in the glass ply and lead their propagation. When the propagation comes closer to the edge of the sample, intra-tows crackings emerge in the carbon plies and each damage quickly propagate in the three plies until the edges of the sample and the break of the glass ply. However, once the glass ply is broken, the carbon plies are cracked but not broken. Indeed, the carbon fibres are not enough loaded. The resin keeps damaging along the band already cracked.

The fibres breakages propagate at a velocity close to the experimental velocity noted in Part I. The curves of fibres breakages length depending on the number of cycles are similar whatever the initial damage size (impact energy) or the imposed displacement (Figure 15). They progress into three steps : an initiation of the propagation, a propagation quite slow and a fast propagation when the damage comes closer to the edges of the sample, due to a structural effect.

The number of cycles required to initiate the damage propagation in the glass ply and the break of the glass ply with the modelling are also close to

values experimentally noted (Tables 7-8).

The post-impact damage propagation scenario explains the influence of the impact energy and the displacement level on the damage initiation and propagation. In fact, the propagation starts with fibres breakages in tension and compression in the glass ply. With a greater initial damage or higher imposed displacement, the glass fibres at the edges of the impacted area deform more easily in tension and compression (Figure 16).

As for the matrix damaging of the carbon plies overtakes the fibers breakages of the glass ply from a certain number of cycles, the final fast evolution of the damage, when it comes closer to the edge of the sample, is lead by the matrix damaging.

5.3. Limitation of the modelling

The semi-continuous modelling is validated for fatigue tensile simulations on carbon/epoxy woven and glass/epoxy woven laminates made up of two identical plies and on the hybrid woven laminate G0C45C45 for which the two carbon plies have the same orientation and no delamination is observed during the experimental fatigue tests. However, a limitation is reached when the two plies have a different orientation and delamination is observed during the experimental tests. For instance, the Figure 17 shows the result of simulations performed on a sample of configuration G0C45C0. First, the modelling manages to obtain two different scenario according the impact energy and the displacement level as for the experimental observation. Even the laminate does not break (after 7.10^6 cycles) : there are only fibers breakages in the glass ply and vertical matrix damaging the lower carbon ply. Even, with the increase of impact energy and displacement level, propagation of

fibres occurs simultaneously in three plies and leads to a rapid failure of the laminate. But, in the first case, the matrix damaging in the carbon ply is not enough developed in comparison to the experimental damaging. This difference is due to the lack of delamination, which has not been implemented yet in the modelling, contrary to what has been done for example in [15].

Nevertheless, the modelling brings an explanation concerning the change of scenario. When the impact energy and the displacement level increases, the fibers of the lower carbon plies are more loaded and fibres breakages can emerge (Figure 18). So, at the experimental level, when the impact energy and the displacement level increase, the fibers breakages propagation can take over the delamination, what leads the failure of the laminate. In the other case, the propagation of delamination between the two carbon plies unload the carbon fibers. So, the resin damaging takes over the fibers breakages.

6. Conclusion

In this article, post-impact fatigue tensile tests have been modeled with the semi-continuous strategy. The modelling manages to represent the propagation of resin damage (tows/resin splittings and intra-tows crackings) in the carbon resin and the propagation of bundles breakages in the glass ply during the fatigue tensile simulation.

The main contribution of this article is to provide a description of a modelling strategy that is able to represent the damage induced by an impact and also the propagation of this damage in fatigue loading with the same model. The original scale and the choice of the damage laws based on experimental observation and on the litterature allows to well represent the physics, the

specific role of the resin and that of the fibres in the behaviour.

In order to do that, the semi-continuous modelling has been extended to fatigue tensile simulations on impacted thin woven carbon/epoxy laminates. The resin damaging is implemented for the shell elements through two fatigue laws $Y_{xy} - N_{resin\,a}$ and $Y_{xy} - N_{resin\,b}$ based on thermodynamical forces. Fiber breakage is introduced through Basquin curves based on tensile and compressive strains for rod elements. Damage accumulation is taken into account by a simple Miner's rule. The strategy is to find in the sample the shell or rod element which requires the lowest number of cycles to reach the breakage and delete it.

The resin fatigue laws have been identified through several simulations on impacted samples of configuration C45C45 and C0C0. The tensile and compressive fiber breakage Basquin curves have been identified through simulations respectively on G0G0 and G0C45C45. The modelling is validated in terms of damage propagation scenario, number of cycles at initiation and speed for mono-material carbon/epoxy and glass/epoxy laminates made up of plies with the same orientation.

It also has been validated for the hybrid configuration G0C45C45. In this case, the modelling can highlight the precise scenario of the post-impact damage propagation. It shows especially that, from a certain number of cycles, the matrix damaging of the carbon plies overtakes the fibers breakages of the glass ply and leads the global propagation of the damage.

However, as the delamination has not been implemented yet, the semi-continuous modelling has not been validated for the configuration G0C45C0, what shows the importance of the delamination consideration in the mod-

elling to correctly represent the post-impact damage propagation. Nevertheless, two different propagation scenario are obtained according the impact energy or the level displacement as for the experimental tests in Part I. When the impact energy and the displacement level increase, fibers breakages can appear in the lower carbon ply oriented at $(0/90)^\circ$. Their propagation can take over the delamination, what leads the failure of the laminate. In the other case, the propagation of delamination between the two carbon plies unload the carbon fibers and the resin damaging is predominant.

Acknowledgment

This work was granted access to the HPC resources of CALMIP supercomputing center under the allocation 2019-P09105.

References

[1] A. Rogani, P. Navarro, S. Marguet, J.-F. Ferrero, C. Lanouette, Tensile post-impact behaviour of thin carbon/epoxy and glass/epoxy hybrid woven laminates – part ii: Numerical study, Composite Structures 230.

[2] S. Miot, Rupture de structures composites stratifiées sous chargements statique et de fatigue, Ph.D. thesis, Université d'Aix-Marseille (2009).

[3] C. Hochard, Y. Thollon, A generalized damage model for woven ply laminates under static and fatigue loading conditions, International Journal of Fatigue 32 (1) (2010) 158 – 165.

[4] R. Talreja, Transverse cracking and stiffness reduction in composite laminates, Journal of Composites Materials 19 (4) (1985) 355–375.

[5] P. Ladevèze, E. LeDantec, Damage modelling of the elementary ply for laminated composites, Composites Science and Technology 43 (3) (1992) 257 – 267.

[6] J. Payan, C. Hochard, Damage modelling of laminated carbon/epoxy composites under static and fatigue loadings, International Journal of Fatigue 24 (2-4) (2002) 299 – 306.

[7] C. Hochard, J. Payan, C. Bordreuil, A progressive first ply failure model for woven ply cfrp laminates under static and fatigue loads, International Journal of Fatigue 28 (10) (2006) 1270 – 1276.

[8] J. Maire, J. Chaboche, A new formulation of continuum damage me-

chanics (cdm) for composite materials, Aerospace Science and Technology 1 (1996) 247–257.

[9] L. Marcin, Modélisation du comportement, de l'endommagement et de la rupture de matériaux composites à renforts tissés pour le dimensionnement robuste de structures, Ph.D. thesis, Université Bordeaux 1 (2010).

[10] T. Rouault, Propagation de coupure en fatigue sur composites tissés : Etude expérimentale et modélisation, Ph.D. thesis, Institut Supérieur de l' Aéronautique et de l' Espace (ISAE) (2013).

[11] M. Miner, Cumulative damage in fatigue, Journal of Applied Mechanics 3 (1945) 159–164.

[12] J. Whitney, R. Nuismer, Stress fracture criteria for laminated composites containing stress concentrations, Journal of Composite Materials 8 (1974) 253–265.

[13] S. Tan, R. Kim, Fracture of composite laminates containing cracks due to shear loading, Exp Mech 28 (1988) 364 – 372.

[14] A. Hillerborg, M. Modéer, P.-E. Petersson, Analysis of crack formation and crack growth in concrete by means of fracture mechanics and finite elements, Cement and Concrete Research 6 (6) (1976) 773–781.

[15] P. Robinson, U. Galvanetto, D. Tumino, G. Bellucci, D. Violeau, Numerical simulation of fatigue-driven delamination using interface elements, Int. J. Numer. Meth. Engng. 63 (2005) 1824–1848.

[16] S. Hallett, B. Green, W. Jiang, M. Wisnom, An experimental and numerical investigation into the damage mechanisms in notched composites, Composites Part A : Applied Science and Manufacturing 40 (5) (2009) 613 – 624.

[17] P. Navarro, F. Pascal, J. Aubry, S. Marguet, J.-F. Ferrero, S. Lemaire, Rauch, Semi-continuous approach for the study of impacts on woven composite laminates: Modeling interlaminar behavior with a specific interface element, International Journal of Impact Engineering 75 (2015) 184 – 193.

[18] F. Pascal, P. Navarro, S. Marguet, Ferrero, On the modelling of low to medium velocity impact onto woven composite materials with a 2d semi-continuous approach, Composite Structures 134 (2015) 302 – 310.

[19] F. Pascal, O. Dorival, P. Navarro, S. Marguet, J.-F. Ferrero, Impact damage prediction in thin woven composite laminates - part i: Modeling strategy and validation, Composite Structures 190 (2018) 32 – 42.

[20] F. Pascal, A. Rogani, B. Mahmoud, P. Navarro, S. Marguet, Ferrero, Impact damage prediction in thin woven composite laminates - part ii: Application to normal and oblique impacts on sandwich structure, Composite Structures 190 (2018) 43 – 51.

[21] A. Rogani, P. Navarro, S. Marguet, J.-F. Ferrero, C. Lanouette, Tensile post-impact behaviour of thin carbon/epoxy and glass/epoxy hybrid woven laminates – part i: Experimental study, Composite Structures 230.

[22] M. Karahan, Investigation of damage initiation and propagation in 2x2 twill woven carbon/epoxy multi-layer composites, Textile Research Journal 81 (4) (2011) 412–428.

[23] A. Bogdanovich, M. Karahan, S. V. Lomov, I. Verpoest, Quasi-static tensile behavior and damage of carbon/epoxy composite reinforced with 3d non-crimp orthogonal woven fabric, Mechanics of Materials 62 (2013) 14 – 31.

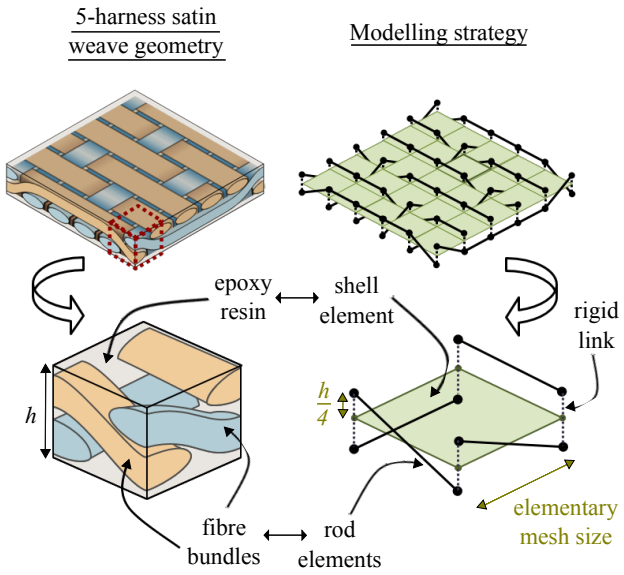

Figure 1: Modelling strategy of the woven ply [1]

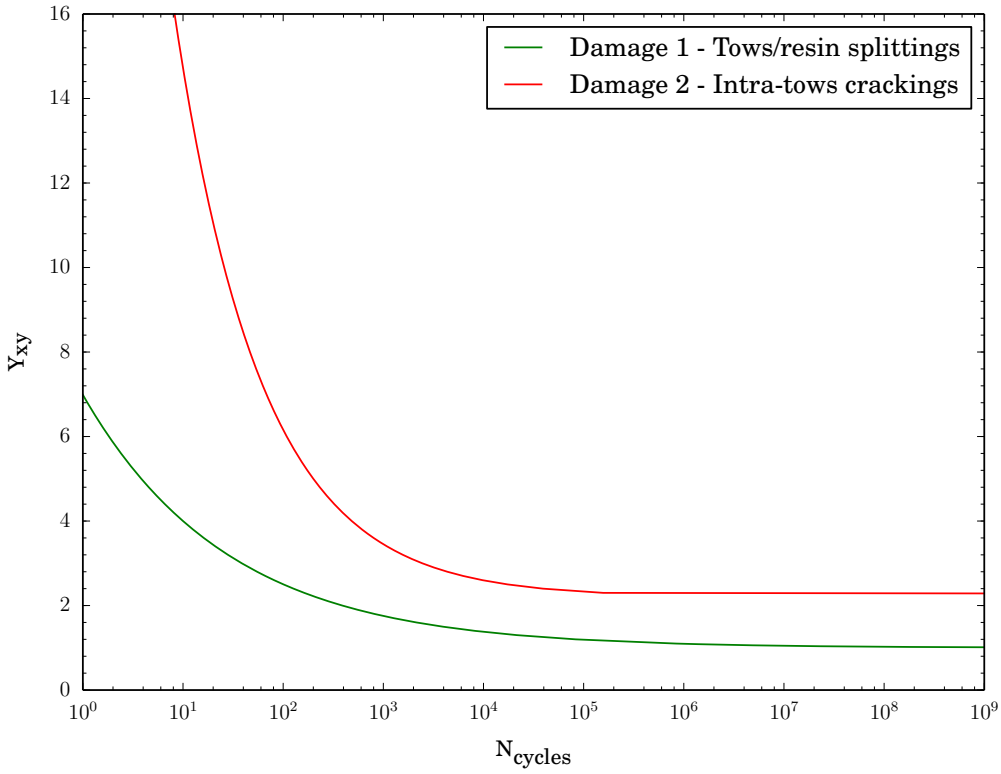

Figure 2: Resin damaging laws identified with fatigue simulations on impacted samples of configuration C45C45 and C0C0

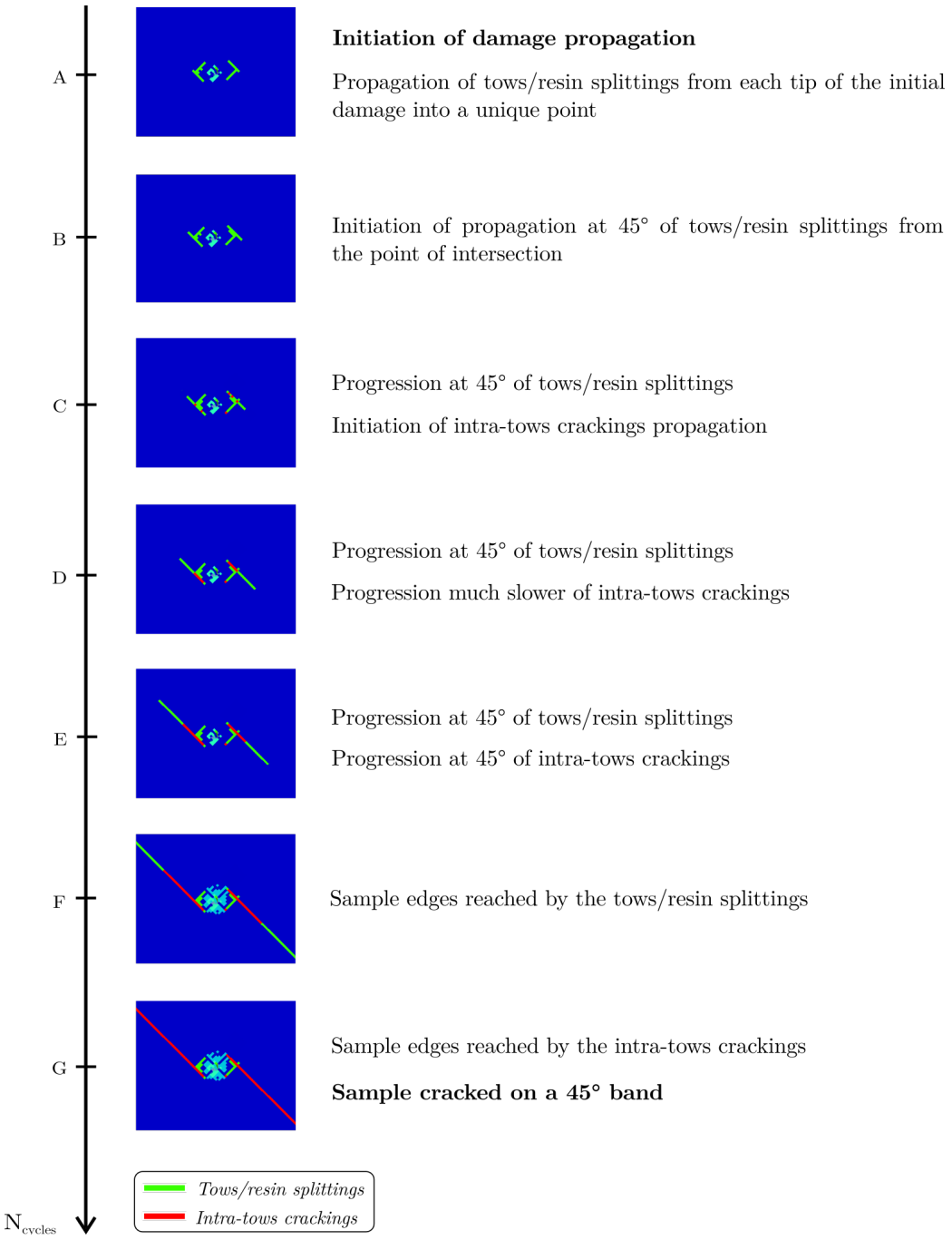

Figure 3: Post-impact damage propagation scenario numerically obtained for the configuration C45C45

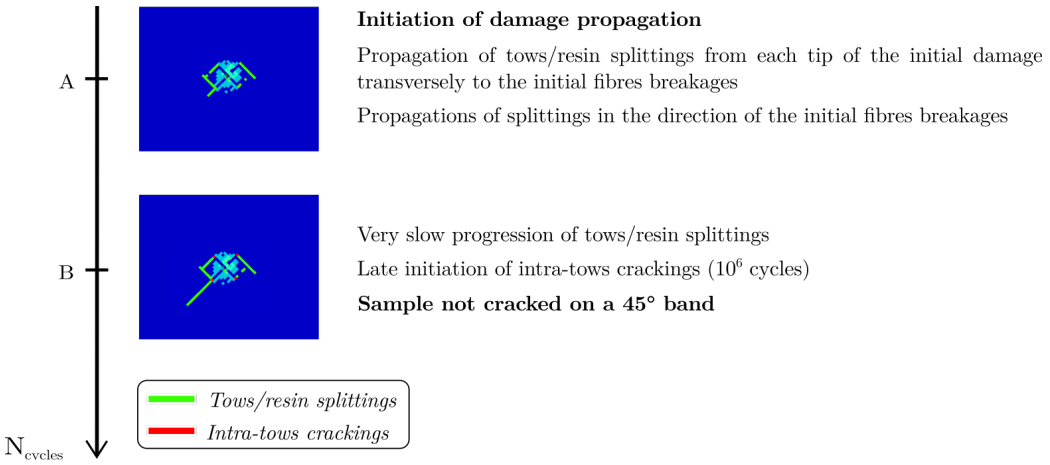

Figure 4: Post-impact damage propagation scenario numerically obtained for the configuration C45C45 subject to the lower impact energy and displacement level

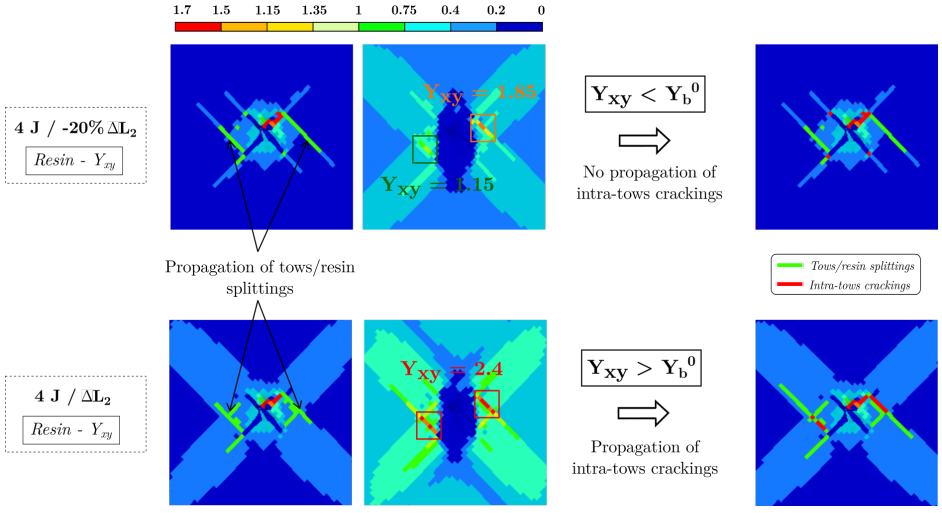

Figure 5: Intra-tows crackings propagation depending on the energy release rate Y_{xy} calculated in the resin for the configuration C45C45

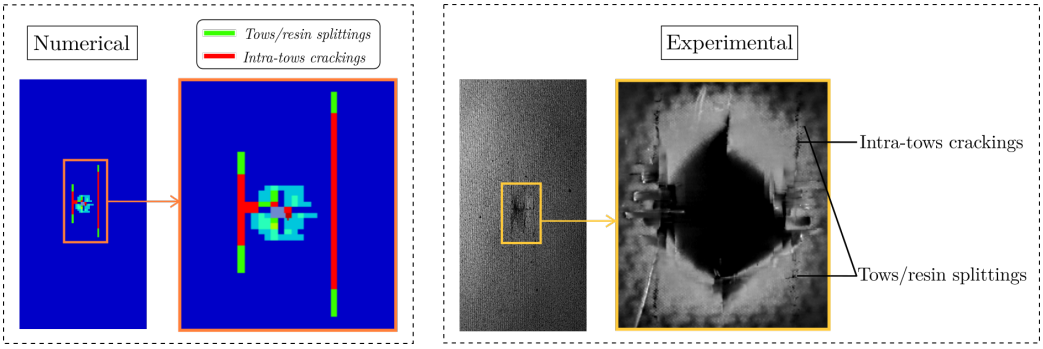

Figure 6: Post-impact damage propagation scenario for the configuration C0C0

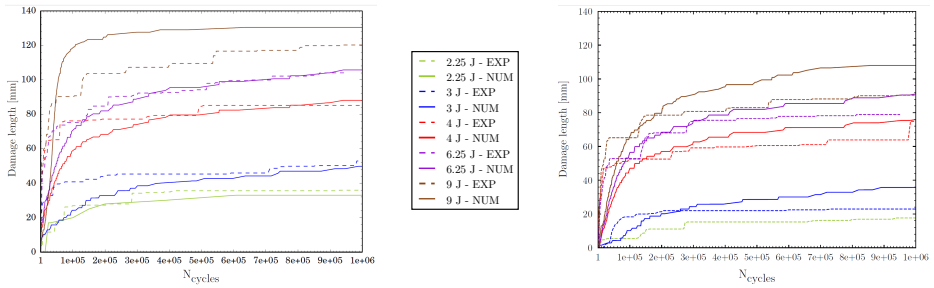

(a) Damage 1 - Influence of impact energy

(b) Damage 2 - Influence of impact energy

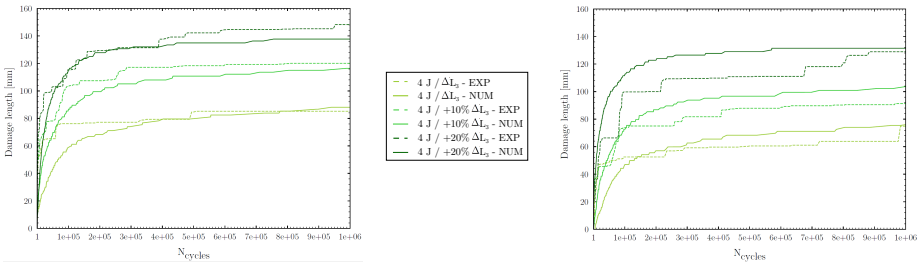

(c) Damage 1 - Influence of displacement level

(d) Damage 2 - Influence of displacement level

Figure 7: Length evolution of the tows/resin splittings (Damage 1) and the intra-tows crackings (Damage 2) depending on the number of cycles for the configuration C0C0

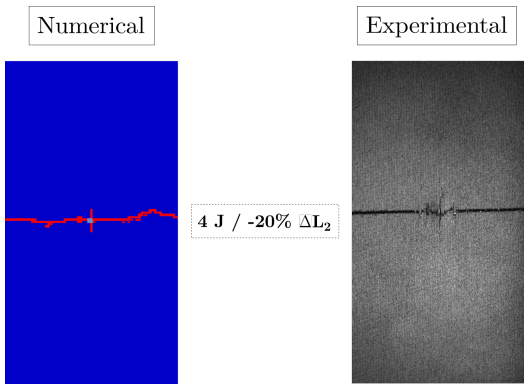

Figure 8: Post-impact damage propagation scenario for the configuration C0C0 for the highest displacement level +30% ΔL_3

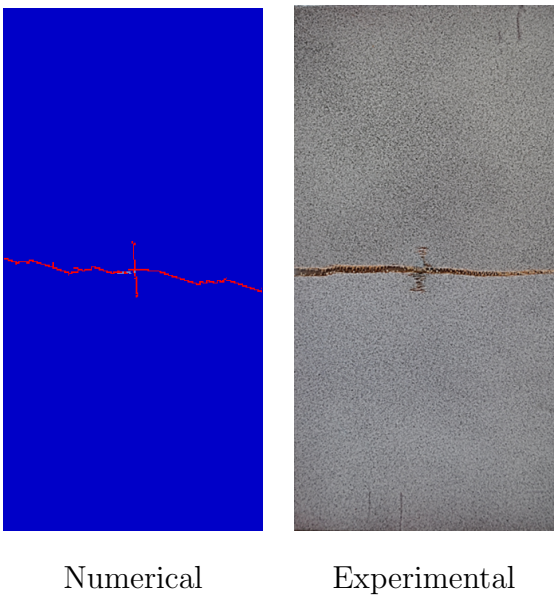

Figure 9: Comparison numerical/experimental of the fracture surfaces obtained after fatigue tension on impacted samples of configuration G0G0

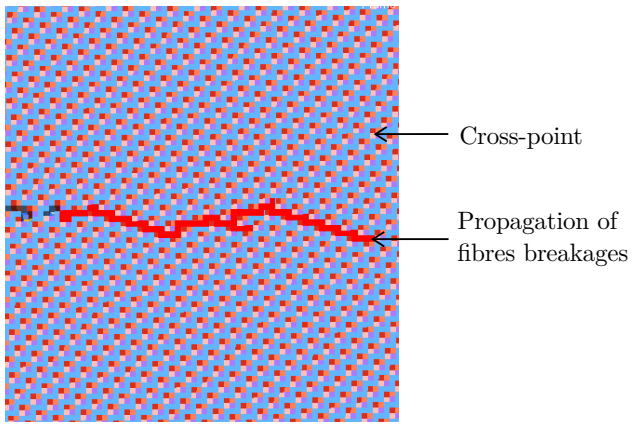

Figure 10: Propagation in fatigue of fibres breakages following the cross-points in a sample of configuration G0G0

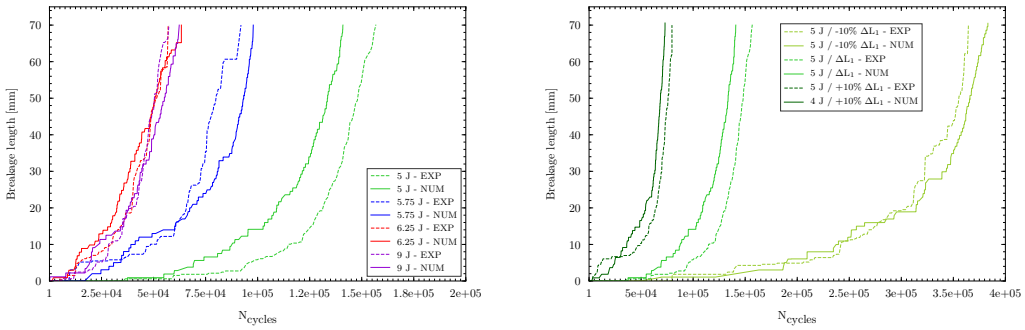

(a) Influence of impact energy

(b) Influence of displacement level

Figure 11: Length evolution of fibres breakages depending on the number of cycles for the configuration G0G0

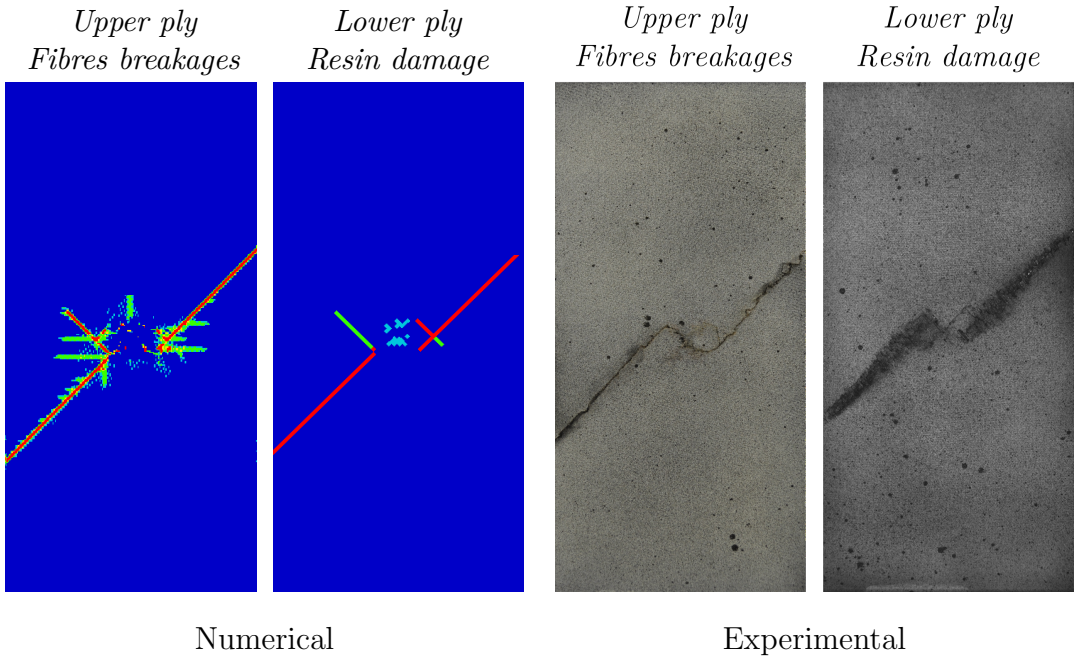

Figure 12: Numerical/experimental comparison of the fracture surfaces obtained after fatigue tension on impacted samples of configuration G0C45C45

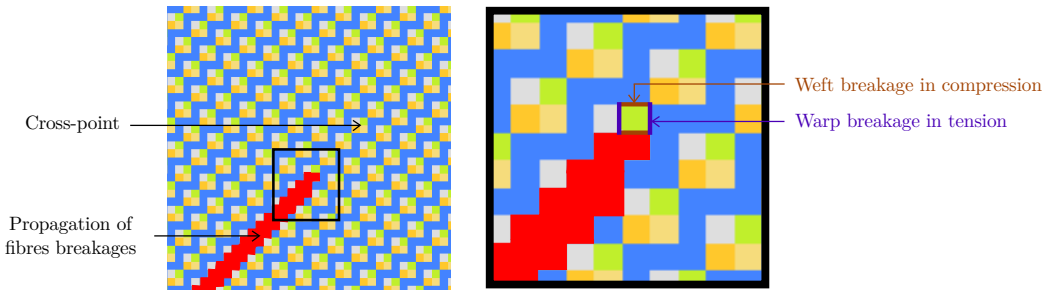

Figure 13: Propagation in fatigue of fibres breakages following the cross-points in the upper glass ply of the configuration G0C45C45

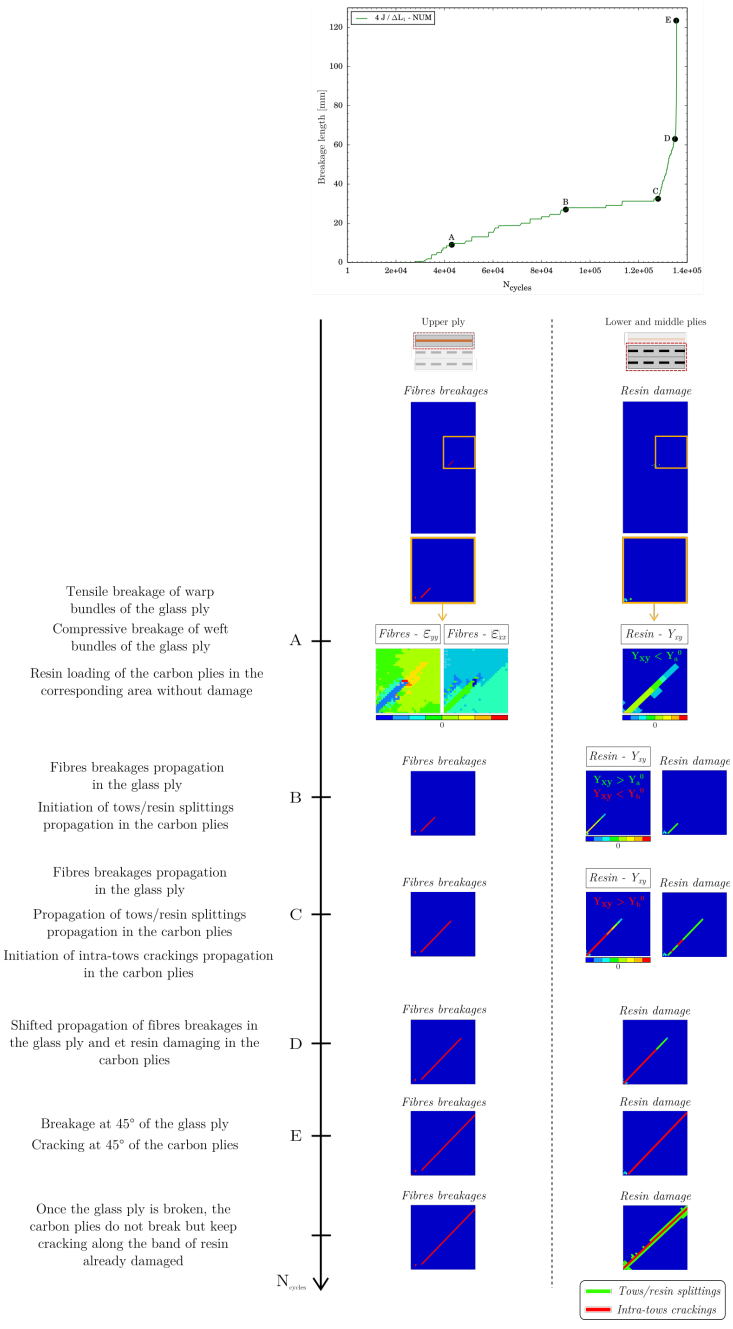

Figure 14: Post-impact damage propagation scenario in fatigue numerically obtained for the configuration G0C45C45

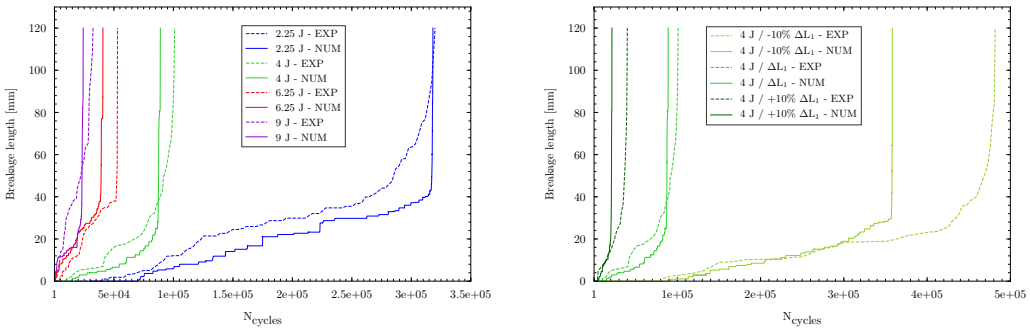

(a) Influence of impact energy

(b) Influence of displacement level

Figure 15: Length evolution of fibres breakages depending on the number of cycles in the upper glass ply of the configuration G0C45C45

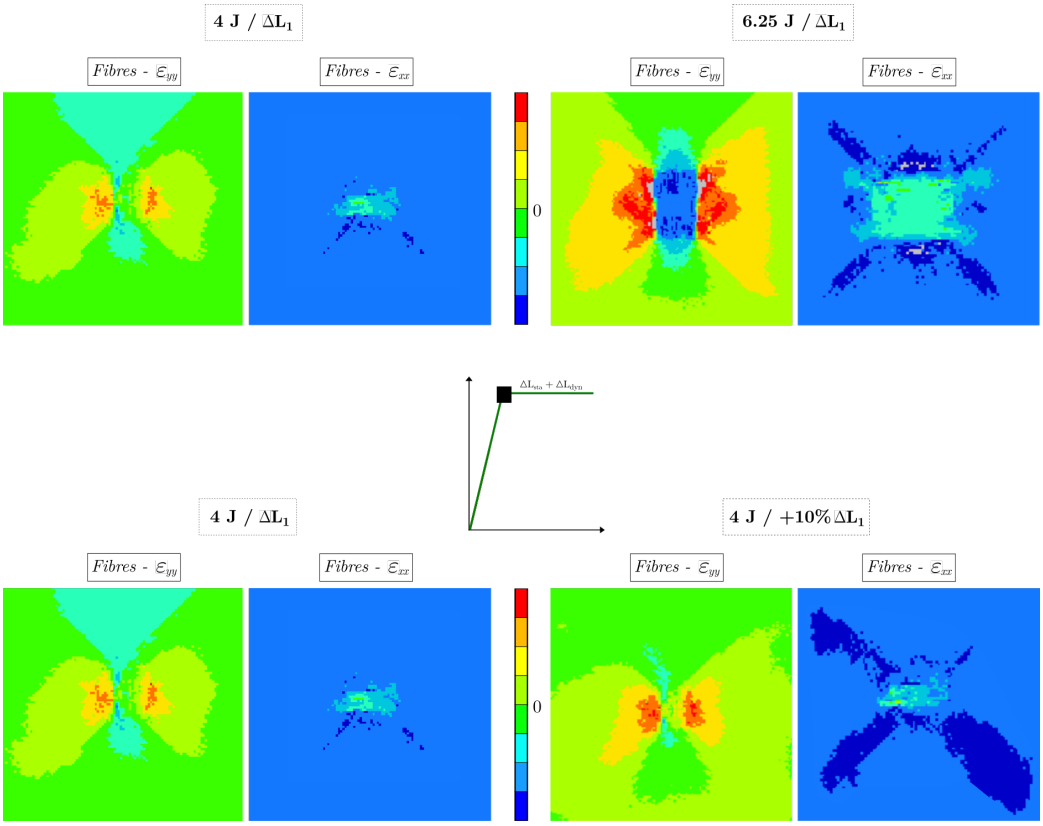

Figure 16: Strain fields ε_{yy} and ε_{xx} at the end of the quasi-static rise of the glass fibres of the configuration G0C45C45 - Influence of the impact energy and the displacement level

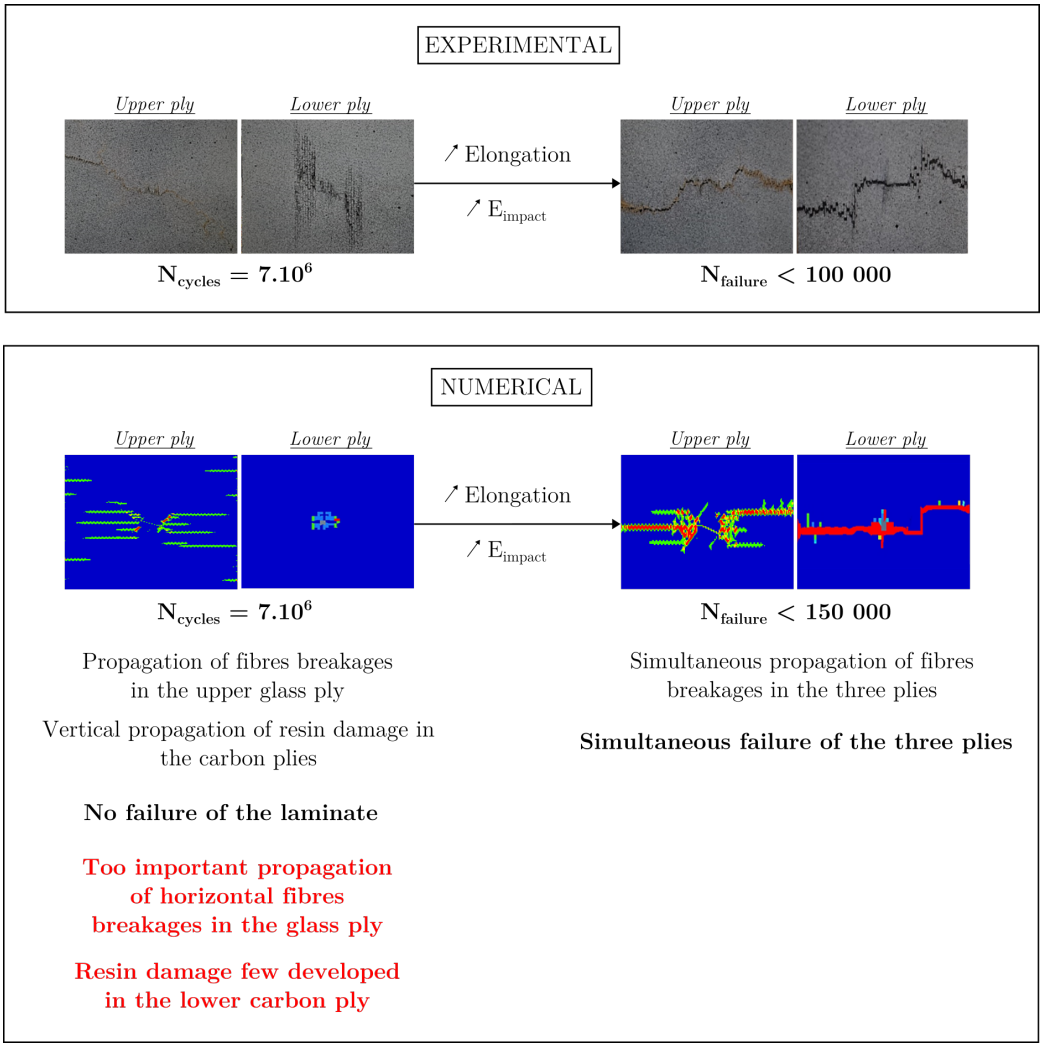

Figure 17: Post-impact damage propagation scenario for the configuration G0C45C0

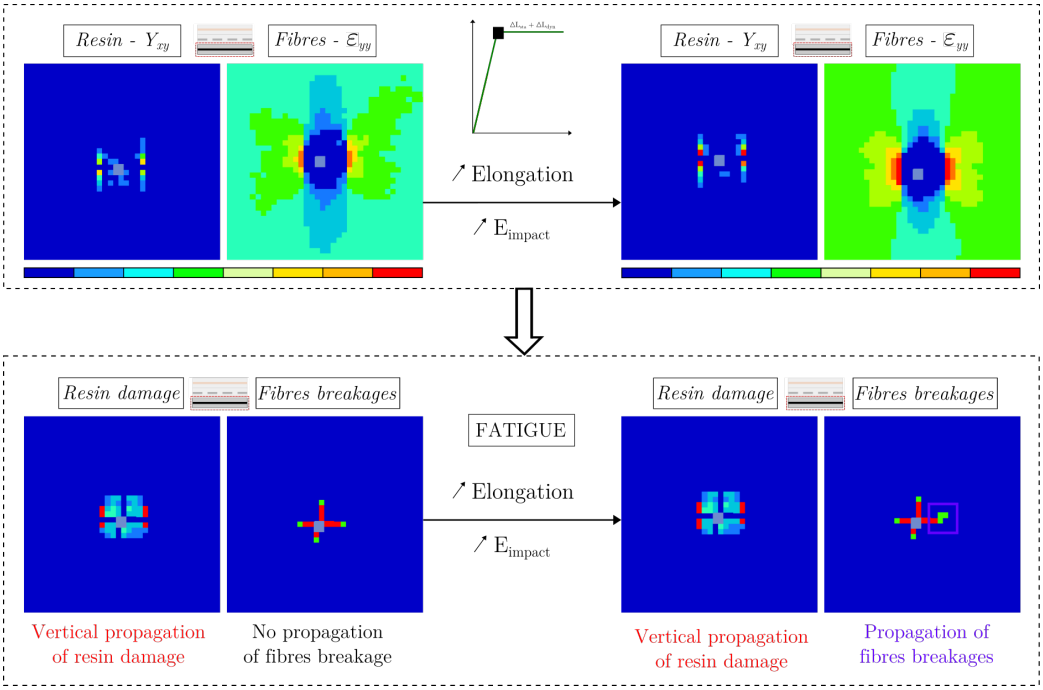

Figure 18: Strain field ε_{yy} and restitution release rate Y_{yy} in the lower carbon ply of the configuration G0C45C0 at the beginning of the fatigue tensile simulation

Configuration	Representation	Upper ply	Lower ply
C0C0		Carbon (0/90)°	Carbon (0/90)°
C45C45	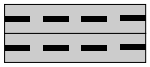	Carbon ±45°	Carbon ±45°
G0G0		Glass (0/90)°	Glass (0/90)°

Table 1: Configurations for single-material laminates [1]

Configuration	Representation	Upper ply	Middle ply	Lower ply
G0C45C45	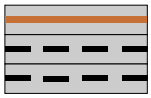	Glass (0/90)°	Carbon ±45°	Carbon ±45°
G0C45C0	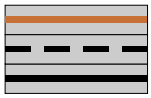	Glass (0/90)°	Carbon ±45°	Carbon (0/90)°

Table 2: Configurations for hybrid laminates [1]

E_{impact}	C45C45 ΔL_2 = 3.01 mm	C0C0 ΔL_3 = 1.04 mm
2.25 J	ΔL_2	ΔL_3
3 J	ΔL_2	ΔL_3
4 J	-20% ΔL_2 ΔL_2 +10% ΔL_2	ΔL_3 +10% ΔL_3 +20% ΔL_3 +30% ΔL_3
6.25 J	ΔL_2	ΔL_3
9 J	ΔL_2	ΔL_3

E_{impact}	G0G0 ΔL_1 = 0.57 mm
5 J	-10% ΔL_1 ΔL_1 +10% ΔL_1
5.75 J	ΔL_1
6.25 J	ΔL_1
9 J	ΔL_1

Table 3: Impact energies and displacement levels used for the fatigue simulations on C45C45, C0C0 and G0G0

E_{impact}	$N_{edges\ EXP}$	$N_{edges\ NUM}$
3 J	120 000	100 000
4 J	60 000	50 000
6.25 J	15 000	8 000
9 J	20 000	10 000

Table 4: Number of cycles necessary to reach the edges of the sample depending on the impact energy for the configuration C45C45

Displacement	$N_{edges\ EXP}$	$N_{edges\ NUM}$
ΔL_2	60 000	50 000
+10% ΔL_2	15 000	12 000

Table 5: Number of cycles necessary to reach the edges of the sample depending on the displacement level for the configuration C45C45

E_{impact}	G0C45C45 $\Delta L_1 = 1.29$ mm
2.25 J	ΔL_1
4 J	-10% ΔL_1 / ΔL_1 / +10% ΔL_1
6.25 J	ΔL_1
9 J	ΔL_1

Table 6: Impact energies and displacement levels used for the fatigue simulations on G0C45C45

E_{impact}	$N_{initiation\ EXP}$	$N_{failure\ EXP}$	$N_{initiation\ NUM}$	$N_{failure\ NUM}$
2.25 J	40 000	320 000	65 000	315 000
4 J	10 000	105 000	12 500	90 000
6.25 J	5 000	55 000	2 000	47 000
9 J	1 000	35 000	500	30 000

Table 7: Number of cycles required to break the glass ply of the configuration G0C45C45 depending on the impact energy

Displacement	$N_{initiation\ EXP}$	$N_{failure\ EXP}$	$N_{initiation\ NUM}$	$N_{failure\ NUM}$
-10% ΔL_1	80 000	480 000	92 000	365 000
ΔL_1	10 000	105 000	12 500	90 000
+10% ΔL_1	4 000	40 000	5 000	25 000

Table 8: Number of cycles required to break the glass ply of the configuration G0C45C45 depending on the displacement level